MRI Measures of Corpus Callosum Iron and Myelin in Early Huntington's Disease

M. Di Paola,[1,2]* O. R. Phillips,[1] C. Sanchez-Castaneda,[3,4] A. Di Pardo,[5] V. Maglione,[5] C. Caltagirone,[1,6] U. Sabatini,[3] and F. Squitieri[5]

[1]*Department of Clinical and Behavioural Neurology, IRCCS Santa Lucia Foundation, Rome, Italy*
[2]*Department of Life, Health and Environmental Sciences, University of L'Aquila, Italy*
[3]*Radiology Department, IRCCS Santa Lucia Foundation, Rome, Italy*
[4]*Department of Psychiatry and Clinical Psychobiology, University of Barcelona, IDIBAPS, Barcelona, Spain*
[5]*Centre for Neurogenetics and Rare Diseases, IRCCS Neuromed (Pozzilli), Italy*
[6]*Neuroscience Department, University of Rome "Tor Vergata", Rome, Italy*

Abstract: Increased iron in subcortical gray matter (GM) structures of patients with Huntington's disease (HD) has been suggested as a causal factor in neuronal degeneration. But how iron content is related to white matter (WM) changes in HD is still unknown. For example, it is not clear whether WM changes share the same physiopathology (i.e. iron accumulation) with GM or whether there is a different mechanism. The present study used MRI to examine iron content in premanifest gene carriers (PreHD, $n = 25$) and in early HD patients ($n = 25$) compared with healthy controls ($n = 50$). 3T MRI acquisitions included high resolution 3D T1, EPI sequences for diffusion tensor imaging (DTI) as an indirect measure of tissue integrity, and T2*-weighted gradient echo-planar imaging for MR-based relaxometry (R2*), which provides an indirect measure of ferritin/iron deposition in the brain. Myelin breakdown starts in the PreHD stage, but there is no difference in iron content values. Iron content reduction manifests later, in the early HD stage, in which we found a lower R2* parameter value in the isthmus. The WM iron reduction in HD is temporally well-defined (no iron differences in PreHD subjects and iron differences only in early HD patients). Iron level in callosal WM may be regarded as a marker of disease state, as iron does not differentiate PreHD subjects from controls but distinguishes between PreHD and HD. *Hum Brain Mapp 35:3143–3151, 2014.* © **2013 Wiley Periodicals, Inc.**

Key words: Huntington's disease; iron; magnetic resonance-based relaxometry; diffusion tensor imaging; white matter; corpus callosum

Contract grant sponsor: Italian Ministry of Health (IMA); Contract grant number: 204/GR-2009-1606835; Contract grant sponsor: European Commission: Marie Curie Fellowship for career development; Contract grant number: FP7-PEOPLE-2011-IEF; Contract grant sponsor: Telethon; Contract grant number: GGP12218; Contract grant sponsor: Marie Curie International Incoming Fellowship; Contract grant number: PIIF-GA-2011-300197; Contract grant sponsors: European HD Network, Lega Italiana Ricerca Huntington (LIRH) ONLUS

*Correspondence to: Margherita Di Paola, Psy. S, IRCCS Santa Lucia Foundation, Via Ardeatina 306, 00179 Rome, Italy.
E-mail: m.dipaola@hsantalucia.it

Received for publication 15 March 2013; Revised 19 July 2013; Accepted 29 July 2013.
DOI 10.1002/hbm.22391
Published online 15 October 2013 in Wiley Online Library (wileyonlinelibrary.com).

INTRODUCTION

Iron is a "biometal" that has a fundamental role in numerous brain metabolic processes, thus it is considered essential for life [Salvador et al., 2011]. In normal conditions, iron concentrations in various regions of the brain vary greatly. In general, regions of the brain associated with motor functions (extrapyramidal regions) tend to have more iron than non-motor-related regions [Koeppen, 1995]; and white matter (WM) stains more strongly for iron than gray matter (GM) [LeVine and Macklin, 1990]. Furthermore, the amount of iron in the brain is is not stable from birth; in fact, it accumulates progressively during brain development [Zecca et al., 2004] and increases until age 40 [Thomas and Jankovic, 2004].

Dysregulation of non-heme iron (ferritin transferring ionic iron) metabolism and its accumulation in various parts of the brain is implicated in the pathogenesis of several neurodegenerative diseases [Moos and Morgan, 2004; Zecca et al., 2004]. Indeed, the presence of higher iron concentrations in subcortical GM structures potentiates reactive oxygen species and consequently contributes to increasing the oxidative stress implicated in neuronal loss in many neurodegenerative disorders, including Huntington's disease (HD) [Bartzokis et al., 1999; Hilditch-Maguire et al., 2000].

How iron content relates to WM changes in HD is still not completely known. It is unclear whether WM changes share the same physiopathology with GM or whether a separate primary pathology/mechanism can explain the WM modifications.

Different from GM, where a variety of cell bodies (neurons, astrocytes, and oligodendrocytes) and processes (axons, dendrites, and myelin) coexist, WM fibers are composed primarily of myelin and axons. Thus, investigating WM allows us to study the process of HD pathogenesis from another prospective (which seems structurally simpler) and to determine how the HD "demyelination hypothesis" [Bartzokis et al., 2007] applies to WM tissue.

According to the HD "demyelination hypothesis", early and heavily myelinated fibers are those most susceptible to myelin breakdown [Bartzokis et al., 2007]. In fact, the breakdown of these fibers is associated with increased density of the oligodendrocytes in the brain, which are involved in repairing the myelin damage. As the oligodendrocytes have the highest iron (ferritin and trasnferrin) content [Bartzokis et al., 2007], when they increase iron content also increases. The consequent iron accumulation is hypothesized to cause further damage (such as oxidative stress) [Beal, 1996]. In this study, we aimed to determine how iron content is linked to WM breakdown in HD.

Iron content can be indirectly measured *in vivo* with transverse relaxation rate (R2*) magnetic resonance imaging (MRI) measures (MR-based relaxometry), known as R2* maps (defined as 1/T2* x 1000). R2* is an MRI measure sensitive to tissue changes (such as changes in iron) and has been shown to be sensitive to iron/ferritin deposits in the brain [Cherubini et al., 2009; Peran et al., 2009]. R2* is not, however, a specific measure of iron; in fact, many other tissue changes, including myelination, calcification, blood flow, and increased tissue water, can influence this measure. To overcome this problem, we used a multimodal MRI approach, combining different MRI acquisitions to differentiate the effects of the main variables (water vs. iron) that can modify R2*.

To date, only two in vivo MRI studies on HD [Bartzokis et al., 2007; Bartzokis and Tishler, 2000] have investigated callosal WM iron content in HD. Both report iron level reduction in frontal WM and in the anterior subregion of the corpus callosum (CC).

In a previous study on macro- and micro-structural callosal modifications in HD [Di Paola et al., 2012], we detected CC volume reduction (macrostructural level) starting in the isthmus; at microstructural level the change was characterized by early WM demyelination accompanied by axonal damage.

In this study, we aimed to continue this line of research [Di Paola et al., 2012]. Specifically, we set out to investigate the physiopathological mechanisms underlying WM callosal changes in a sample of HD patients. We wished to determine whether the macro- and microstructural callosal WM changes found in HD are related to modifications in R2* and whether CC R2* is a possible marker of the disease state by comparing premanifest gene carriers (PreHD) with healthy subjects (HC) and patients in the early stages of HD (i.e., I and II). For this purpose, we combined two well-validated macro- and micro-structural analysis techniques: voxel-based morphometry (VBM) to map callosal WM density and diffusion tensor imaging (DTI) to investigate microstructural differences in callosal WM. We also used a relatively new MRI technique, namely, voxel-based relaxometry (VBR). This is a morphometric method that analyzes R2* maps on a voxel-by-voxel basis, with no a priori selected region of interest.

MATERIALS AND METHODS

Subjects

Demographic and clinical characteristics of the sample are presented in Table I. All HD subjects (n = 50) underwent a genetic test (abnormal CAG repeats >36) and were examined clinically by the same neurologist with expertise in HD. Twenty-five PreHD subjects and 25 HD patients in the early disease stages (I and II) were enrolled in the study. All individuals were assessed using the Unified Huntington's Disease Rating Scale (UHDRS), which includes motor, cognitive, behavioral, and functional subscales [Huntington et al., 1996]. Each section consists of a multistep subscale. The motor section measures eye movements, limb coordination, tongue impersistence and movement disorders (such as rigidity, bradykenisia, dystonia,

TABLE I. Sociodemographic and clinical characteristics of patients and control subjects

Characteristics	PreHD (n = 25)	PreHD Cnt (n = 25)	HD (n = 25)	HD Cnt (n = 25)	Fisher's Exact Test; F or T Test	df	P
Gender male/female	16/9	16/9	14/11	14/11	0.719	3	0.907
Age (years + SD)	37.44±7.01	37.32±7.12	47.40±14.53	48.44±14.25	7.237	3	$0.015^{a\dagger\dagger}$; $0.005^{b\dagger\dagger}$
CAG repetition length	43.28±2.17	NA	46.68±6.80	NA	−2.380	48	$0.021^{a\dagger\dagger}$
MMSE	27.82±1.24	NA	24.97±3.23	NA	3.682	38	$0.001^{c\dagger\dagger}$
UHDRS Motor	8.00±9.28	NA	37.22±13.18	NA	−8.695	44	$0.001^{a\dagger\dagger}$
UHDRS Cognitive	257.80±42.34	NA	142.65±50.35	NA	8.046	41	$0.001^{c\dagger\dagger}$
UHDRS Behavioral	7.67±7.84	NA	18.39±9.13	NA	−4.160	42	$0.001^{a\dagger\dagger}$
UHDRS Functional	25 + 0	NA	17.91±5.68	NA	5.984	44	$0.001^{c\dagger\dagger}$
TFC	13 + 0	NA	8.39±2.37	NA	9.329	44	$0.001^{c\dagger\dagger}$
Indipendence scale	99.80 + 1.04	NA	78.04±12.49	NA	8.312	44	$0.001^{c\dagger\dagger}$
Disease burden	292.3±87.52	NA	458.6±104.75	NA	−6.091	48	$0.001^{a\dagger\dagger}$

HD, Huntington's disease; PreHD, gene-positive, without motor symptoms; PreHD Cnt, control subjects for Pre-HD; HD Cnt, control subjects for HD; SD, standard deviation; df, degrees of freedom; CAG, trinucleotide repeat number; MMSE, Mini Mental State Examination; UHDRS, Unified Huntington's Disease Rating Scale; TFC, Total Functional Capacity; NA, not available; ††T-student, Bonferroni correction.

[a]PreHD < HD (when referred to a cognitive scale comparison or CAG repetition, higher punctuations mean greater impairment).

[b]PreHD Cnt < HD Cnt.

[c]PreHD > HD (when referred to a cognitive scale comparison, higher punctuations mean lesser impairment).

*MMSE: Missing data for 5 PreHD subjects & 5 HD patients.

*UHDRS Motor: Missing data for 2 PreHD subjects & 2 HD patients.

*UHDRS Cognitive: Missing data for 5 PreHD subjects & 2 HD patients.

*UHDRS Behavioral: Missing data for 4 PreHD subjects & 2 HD patients.

*UHDRS Functional: Missing data for 2 PreHD subjects & 2 HD patients.

*TFC: Missing data for 2 PreHD subjects & 2 HD patients.

*Indipendence scale: Missing data for 2 PreHD subjects & 2 HD patients.

chorea, and gait disturbances). The cognitive scale mainly evaluates executive function. The behavioral section investigates the presence of depression, aggressiveness, obsessions/compulsions, delusions/hallucinations and apathy. The functional assessments include the HD functional capacity scale (HDFCS), the independence scale and a checklist of common daily tasks. All three scales mainly investigate independence in daily life activities. The HDFCS is reported as the total functional capacity (TFC) score (range 0–13) and is the only functional subscale with established psychometric properties (including inter-rater reliability and validity), which are based on radiographic measures of disease progression. Thus, the TFC score is used worldwide to determine patients' HD stage. On the independence scale, the investigator indicates whether the patient can perform the task that evaluates independence level (range 10–100). The checklist (functional assessment) is summed by giving a score of 1 to all "yes" answers (range 0–25). Pre-HD subjects included asymptomatic ones (total motor score <5 on the UHDRS) [Paulsen et al., 2001]. The Disease Burden index, a measure of disease severity, was used according to the already described formula (age × [CAG-35.5]), where CAG is the number of CAG repeats [Penney et al., 1997]. The Mini-Mental State Examination (MMSE) [Folstein et al., 1975], which measures global cognitive functioning, was administered to PreHD subjects and HD patients. Patients in the advanced stages of disease (Stages III and IV) and/or with traumatic brain injury or MRI focal lesions were excluded.

We recruited 50 HC from the community. They were individually age- and sex-matched with the PreHD subjects and HD patients. Consent was obtained from all participants according to the Declaration of Helsinki. The study was approved by the Santa Lucia Foundation Research Ethics Committee.

MRI Data Acquisition

All MRI data were acquired with a 3T Allegra MRI system (Siemens, Erlangen, Germany) using a birdcage head coil.

As in our previous study [Di Paola et al., 2012], scans were collected in a single session with the following pulse sequences: (a) proton density (PD) and T2-weighted double turbo spin-echo (SE) sequences acquired in transverse planes (TR: 4500 ms, TE: 12 ms, TE: 112 ms, FOV 230×172 mm, matrix 320×240, slice thickness: 5 mm, number of slices: 24); (b) fluid-attenuated inversion-recovery (FLAIR) sequences in the same planes as the SE sequences (TR/TE/TI: 8500/109/2000 ms; FOV: 230×168 mm, matrix: 256×256, slice thickness: 5 mm, number of slices: 24); (c) T1-weighted 3D images, with partitions acquired in the sagittal plane, using a modified driven equilibrium Fourier transform (MDEFT) [Deichmann et al., 2004] sequence

(TE/TR/TI: 2.4/7.92/910 ms, flip angle: 15 degrees, 1 mm^3 isotropic voxels); (d) diffusion-weighted volumes were also acquired using spin-echo echo-planar imaging (TE/TR: 89/8500 ms, bandwidth: 2126 Hz/vx; matrix: 128x128; 80 axial slices, voxel size: 1.8x1.8x1.8 mm) with 30 isotropically distributed orientations for the diffusion sensitizing gradients at a *b*-value of 1,000 s/mm^2 and 6 $b = 0$ images. Scanning was repeated three times and averaged to increase the signal-to-noise ratio; (e) and six consecutive T2*-weighted gradient echo-planar imaging sequences at different echo times (TE) (TEs: 6, 12, 20, 30, 45 and 60 ms; TR =5,000; bandwidth = 1116 Hz/vx; matrix size 128 x 128 x 80; flip angle 90°; voxel size of 1.5 x 1.5 x 2 mm^3) [Cherubini et al., 2009; Peran et al., 2009].

Callosal WM Density Analysis (VBM Approach)

Images were processed and analyzed using VBM [Ashburner and Friston, 2000; Good et al., 2001] in the statistical parametric mapping framework (SPM5, Wellcome Department of Imaging Neuroscience, University College London, UK) (for technical Details see Di Paola et al., 2012).

We applied independent sample *t*-tests using the WM partitions (unmodulated data, 8 mm smoothed) to compare groups (PreHD subjects vs. controls; HD patients vs. controls and PreHD subjects vs. HD patients). Statistical maps were corrected for multiple comparisons by controlling the false discovery rate (FDR) at 5% ($P < 0.05$).

Callosal MD, FA, AD, and RD Analysis (TBSS Approach)

Diffusion-weighted images were processed with the FMRIB Software Library (FSL 4.1 www.fmrib.ox.ac.uk/fsl/). We generated fractional anisotropy-FA, mean diffusivity-MD, axial diffusivity-AD, and radial diffusivity-RD maps. Then we used TBSS [Smith et al., 2006], version 1.2, which is part of the FSL software package, for post-processing and analysis of the multi-subject DTI data [for all technical details see Di Paola et al, 2012].

To test for localized differences across groups (PreHD subjects vs. controls; HD patients vs. controls; PreHD subjects vs. HD patients), voxelwise statistics were performed for each point on the common FA skeleton. A permutation-based approach [Nichols and Holmes, 2002], which accounts for family-wise errors (FWE), was used to control for multiple comparisons ($P < 0.05$).

Callosal R2* Measurement (Voxel-Based Relaxometry Approach)

The R2* data were pre-processed according to Specht et al.'s [2005] protocol. After defining the anterior commissure in each image as the origin of the individual stereotaxic space, we reoriented all images to the axial view.

First, we segmented (New segment tool in SPM8) only those T2* images that were acquired with an echo time of TE 60 ms. These images gave the best GM–WM differentiation, which is relevant for the automated segmentation procedure [Ashburner and Friston, 2000]. Then, we normalized only WM segments. The resulting WM transformation was applied to the R2* image of the respective subject. All R2* images were resampled with a voxel size of 2 x 2 x 2 mm^3 and the same extended bounding-box as used for the T1 images. To obtain optimally normalized R2* images, we created a new R2* template by averaging all normalized R2* images across both groups. This average image was smoothed with a Gaussian kernel of 8-mm FWHM [Good et al., 2001], which is the assumed smoothness of the templates, as used in SPM. Then, the original, non-normalized R2* maps were directly normalized into the MNI space using the new R2* template.

This procedure resulted in normalized R2* images without the need for additional segmentation. Therefore, we smoothed the normalized images using a Gaussian kernel of 8 mm full width at half maximum (FWHM) and entered the images into subsequent statistical analyses.

To analyze the R2* maps, we applied independent sample *t*-tests at each voxel to compare groups (PreHD subjects vs. controls; HD patients vs. controls and PreHD subjects vs. HD patients). Statistical maps were corrected for multiple comparisons by controlling the false discovery rate (FDR) at 5% ($P < 0.05$).

RESULTS

Demographic and Clinical Characteristics

The PreHD subjects and HD patients did not differ from their respective control groups for age or sex (see Table I). There were also no differences in sex between PreHD subjects and HD patients; however, these groups differed in age and CAG repetition length. As expected, HD patients performed significantly worse on all measures assessed by the UHDRS (see Table I) and also a significantly higher score at Disease Burden (see Table I).

We entered age as a covariate in each statistical analysis that compared PreHD subjects versus HD patients.

Callosal WM Density Analysis (VBM Approach)

As shown in Figure 1 (Panel A), when PreHD subjects were compared with healthy controls, no significant callosal WM density difference emerged (the result in the figure did not survive after FDR correction $P < 0.05$).

When PreHD subjects were compared with HD patients (Panel B), the callosal WM density of the latter was lower mainly in the isthmus but also anteriorly in the body and posteriorly in the splenium. When HD patients were compared with healthy controls (Panel C), a significant WM

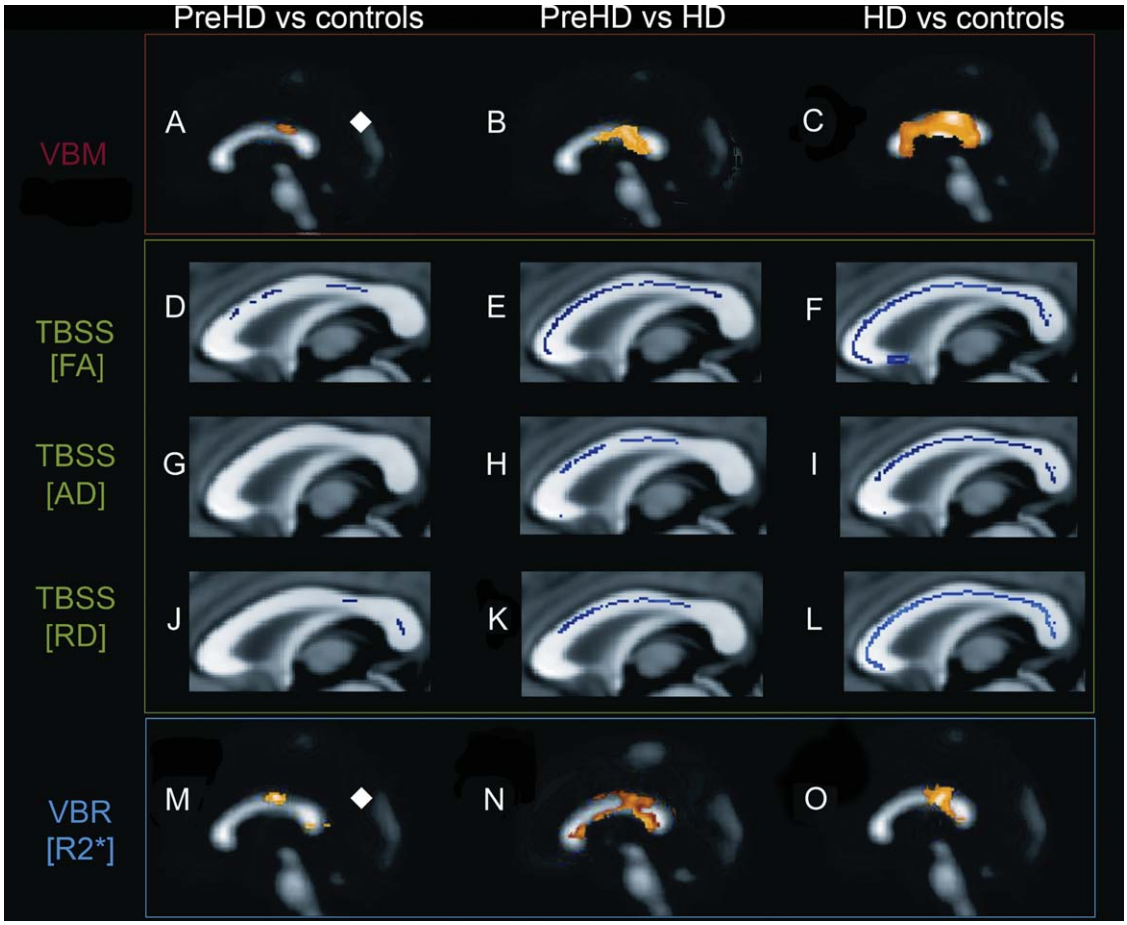

Figure 1.

Structural changes and iron content in PreHD subjects and HD patients. The left panels show results of the comparison between PreHD and controls. The central panels show results of the comparison between PreHD and HD. The right panels show results of the comparison between HD and controls. The top panels show results of the VBM analysis. The middle panels show results of the DTI analysis (FA, AD, RD parameters). The bottom panels show results of the VBR analysis (R2* parameter). Compared with controls, PreHD patients show no significant changes in WM density in the CC (Panel A); reduced fractional anisotropy (FA) in the isthmus and anterior callosal body (Panel D); no changes in AD (Panel G); increased radial diffusivity (RD) in the isthmus and splenium (Panel J); no significant changes in R2* value (Panel M). Compared with PreHD, HD patients show reduced WM density in the splenium, isthmus and posterior callosal body (Panel B); reduced FA in the isthmus, callosal body and genu (Panel E); increased AD in the callosal body (Panel H); increased RD in the isthmus and callosal body (Panel K); reduced R2* value in the splenium, isthmus, posterior callosal body and rostrum (Panel N). Compared with controls, HD patients show reduced WM density across almost the entire CC (Panel C); reduced FA across the whole CC (Panel F); increased AD in the splenium, isthmus and callosal body (Panel I); increased RD across the whole CC (Panel L); and a reduced R2* value in the splenium and isthmus (Panel O). ◆: results that did not survive after statistical correction FDR $P < 0.05$.

density reduction was found involving the CC as a whole (see Figure 1).

Callosal FA, MD, AD, and RD Analysis (TBSS Approach)

As shown in Figure 1, the spatial distribution of differences between PreHD and controls on DTI parameters was as follows: (1) FA was lower in the isthmus and in the anterior body of the CC in PreHD subjects (Panel D); (2) there was no significant difference in AD and MD between groups (Panel G; MD data not shown); and (3) RD was greater in the isthmus and splenium of the CC in PreHD subjects (Panel J).

The spatial distribution of differences between PreHD subjects and HD patients on DTI parameters was as

follows: (1) FA was lower in the isthmus, callosal body and genu in HD patients (Panel E); (2) AD and MD were higher in the callosal body in HD patients (Panel H; MD data not shown); and (3) RD was higher in the isthmus and callosal body in HD patients (Panel K).

The spatial distribution of differences between HD patients and control subjects on DTI parameters was as follows: (1) FA was lower in all CC regions in HD patients (Panel F); (2) AD was higher in the splenium, isthmus and callosal body in HD patients (Panel I) and MD was higher in all CC regions (data not shown); and (3) RD was higher in all CC regions in HD patients (Panel L).

Callosal R2* Measurement (Voxel-Based Relaxometry Approach)

As shown in Figure 1 (Panel M), when PreHD subjects were compared with healthy controls, we did not detect any significant R2* difference (the result in the figure did not survive after FDR correction $P < 0.05$). When PreHD subjects were compared with HD patients (Panel N), the callosal R2* value in HD patients was lower mainly in the isthmus but also more anteriorly, involving the callosal body and the rostrum, and more posteriorly in the splenium. When HD patients were compared with healthy controls (Panel O), we found a significantly reduced callosal R2* value in the isthmus (see Figure 1).

DISCUSSION

Iron is an essential "biometal" that is vital in cell functions [Salvador et al., 2011]. During development, it accumulates progressively in the brain [Zecca et al., 2004]. In normal conditions, oligodendrocytes are the principal cells in the central nervous system that stain for iron. Both human and animal studies [Todorich et al., 2009] have shown that chronic severe iron deficiency leads to hypomyelination. This finding supports the role of this biometal in myelin production.

The "demyelination hypothesis" [Bartzokis et al., 2007] suggests that the breakdown of early and heavily myelinated fibers is associated with increased density of oligodendrocytes attempting to repair myelin damage. As the oligodendrocytes have the highest iron content of all brain cell types [Bartzokis et al., 2007], an increase in their number causes an increase in iron. This iron accumulation is hypothesized to cause further damage (such as oxidative stress) [Beal, 1996]. Indeed, the dysregulation of iron metabolism and accumulation in various parts of the brain is implicated in the pathogenesis of several neurodegenerative diseases, including HD [Moos and Morgan, 2004; Zecca et al., 2004]. This mechanism is well known in HD subcortical GM structures, where increased iron has always been reported [Sanchez-Castaneda et al., 2013; Vonsattel et al., 2008]. In this study, we aimed to investigate the relationship between WM breakdown and iron, as measured by the R2* parameter.

Our first finding was loss of R2* in the callosal WM in HD, which highlights a new aspect: the R2* in HD has a different pattern at the WM level (decreased R2*) and at the GM level (increased R2*).

One possible explanation of our results comes from animal model studies that found differences in iron accumulation in WM and GM based on different iron metabolism/accumulation in WM versus GM oligodendrocytes. Indeed, WM oligodendrocytes have been found to be equipped with additional iron efflux mechanisms to prevent intracellular iron overload, a compensatory upregulation that likely works as a fail-safe mechanism [Schulz et al., 2011].

Second, we found that the R2* change in callosal WM in HD is temporally well-defined: myelin breakdown starts in the PreHD stage, with no R2* changes, and R2* reduction manifests only in the early HD stage. This finding can be explained by referring to Bartzokis et al.'s hypothesis [2012]. Specifically, the HD brain may be continually trying to remyelinate in a losing attempt to compensate for the disease-related myelin loss. In HD, these remyelination processes may successfully compensate in the early years, which usually correspond to the beginning of the pathology, or in the years prior to onset. But, eventually they start to fail in later years as brain myelin volume continues to grow and it becomes increasigly difficult to maintain this expanding volume. The critical point of the remyelination failure may vary depending on the CAG repeat length.

Third, we suggest that as the R2* does not differentiate subjects prior to disease onset (PreHD) from controls, but distinguishes between PreHD subjects and patients in the earliest stages of HD, the callosal R2* level should be regarded as a marker of disease state.

Although R2* is an MRI measure sensitive to tissue changes (such as iron changes), it is not a specific measure of iron. In fact, many other tissue changes, including myelination, calcifications, blood flow, and increased tissue water, can influence this measure. Briefly, R2* is an MRI measure of microscopic magnetic field inhomogeneity. It is increased by the paramagnetic effect of iron and the diamagnetic effect of myelin. In other words, as tissue iron and deoxyhaemoglobin are paramagnetic, when placed in an external magnetic field their magnetic moment aligns along the field, causing a slight increase in magnetic field strength and intra-voxel field inhomogeneity; thus, an increase in tissue iron, or deoxyhaemoglobin (from increased oxidative metabolism) will increase R2* [Yablonskiy and Haacke, 1994]. On the other side, myelin is diamagnetic; when placed in an external magnetic field its intrinsic magnetic moment aligns against the field, causing a decrease in magnetic field strength but also an increase in magnetic field inhomogeneity [He and Yablonskiy, 2009]. Thus myelin also increases R2* [Li et al., 2012].

In this study, by combining different MRI acquisitions (DTI and R2*) we were able to differentiate the effects of the main variables (water vs. iron) that can modify R2*. Thus, we believe it is very likely that many of the R2*

differences which emerged in our study were due to iron modifications.

From a methodological point of view, combining different MRI acquisitions is the novelty of this study. We acquired MRI R2* parameters in conjunction with different DTI parameters (FA, MD, RD, and AD). Together, they allowed us to explore microstructural differences in the callosal WM changes of our patients and to investigate the potential role of different underlying mechanisms (demyelination vs. iron content) and factors (water vs. iron). Furthermore, different from previous studies [Bartzokis et al., 2007; Bartzokis and Tishler, 2000] we did not use a priori selection of a brain region to detect iron content.

In agreement with previous studies [Di Paola et al., 2012; Rosas et al., 2010], we found that the isthmus was the CC sub-region most affected in PreHD subjects. Our DTI analysis detected FA and RD differences only in the isthmus of PreHD subjects. Furthermore, again in agreement with the mentioned studies, we found no significant AD difference in PreHD. This suggests the occurrence of myelin damage in the presymptomatic stages, not impaired axonal coherence. We found no WM density changes or iron content differences in PreHD as compared with controls. This suggests that significant WM demyelination occurs prior to iron and volumetric modifications.

In HD patients, the whole CC showed decreased WM density compared with controls, in agreement with the findings of previous studies [Hobbs et al., 2010; Rosas et al., 2010]. FA, AD, and RD were also significantly different in all CC regions in HD patients compared with controls. These findings suggest that both myelin breakdown (reflected by increased RD) and axonal damage (reflected by increased AD) can affect callosal WM when HD is fully manifested. When HD patients were compared with healthy controls, we found a significantly reduced callosal R2* value mainly in the isthmus.

Comparisons between PreHD subjects and HD patients also suggest that CC changes are temporally and spatially well defined. Modifications seem to be detectable in the isthmus in PreHD subjects and proceed in a posterior-to-anterior direction, eventually involving both the isthmus and body of HD patients for all parameters investigated (i.e., callosal WM density, myelin and axonal integrity and iron content).

Results of comparisons between PreHD subjects and HD patients confirm that the difference in the isthmus of PreHD subjects is most likely caused by specific damage to the myelin sheaths (i.e., we observed changes in RD but not AD). In later HD stages (I and II), these alterations seem to be driven by both myelin and axonal damage (i.e., in HD patients we observed changes in both RD and AD). The callosal R2* value of HD patients was lower than that of pre-HD subjects mainly in the isthmus, but also more anteriorly involving the callosal body and the rostrum and posteriorly, the splenium.

The finding of reduced R2* in callosal WM is in agreement with two previous studies in the literature [Bartzokis et al., 2007; Bartzokis and Tishler, 2000]. In both, the Authors reported a decreased iron level in the frontal lobe WM and anterior CC using the field dependent relaxation rate (FDRI) method which compares the R2 values calculated from spin-echo images obtained at lower- and higher-field strengths to obtain a measure of iron in ferritin deposits. The low field-strength instrument R2 is highly sensitive to MR-visible water and it showed increased MR-visible water in the same WM regions. The Authors concluded that in these regions their results might have been due to decreased iron or increased MR-visible water caused by tissue damage.

Applying what we mentioned above about the R2* changes to our results, it seems that reduced R2* may be due to tissue loss and consequently increased water and/or reduced tissue iron. Although we have no other direct measures (such as phase images) to help us discriminate between the roles of iron and water, we can use the DTI parameters as indirect measures to exclude the potential confounding effects of water. In PreHD versus controls, we found early WM demyelination with no difference in R2*. In the HD versus PreHD comparison, we found that demyelination at the level of the isthmus was more anteriorly associated with axonal damage. We also found reduced R2* at the level of the isthmus, with no difference in MD in the same callosal subregion. Thus, as no differences in the total amount of water in the isthmus were present (i.e., no difference in MD), we can infer that the difference we found in R2* in the isthmus was more likely due to reduced iron content.

Thus, we suggest that the reduced iron level had a main effect on our results. Of course, as the pathology progresses it is likely that both iron and water will be present and affect WM callosal changes.

Before drawing conclusions some limitations of the present study should be acknowledged. First longitudinal studies need to be performed to investigate the evolution of the brain changes in HD over the time. Second, larger PreHD and HD samples need to be collected to better assess the influence of CAG repeats. Third a group of PreHD soft signs should be included in the future studies, to further investigate the pre-symptomatic stage of HD. The PreHD soft signs can be indeed considered as an intermediate pathology stage between the pre-symptomatic subjects (PreHD) and the symptomatic patients (HD). Four a blinded region of interest analyses should be run to confirm automated analyses findings.

CONCLUSIONS

In agreement with the HD "demyelination hypothesis" [Bartzokis et al., 2007], we found the breakdown of early and heavily myelinated fibers, such as those present in the isthmus. Furthermore, in agreement with the same Authors [Bartzokis et al., 2007; Bartzokis and Tishler, 2000], we found reduced iron in the callosal WM.

Thus, in HD the pattern of iron content seems to be characterized by decreased iron in WM and increased iron

in subcortical GM. One possible explanation of this result comes from an animal model study. Schulz et al. [2011] reported that oligodendrocytes seem to be equipped with an additional iron efflux fail-safe mechanism.

Whether the reduced iron content is related to a neurodegenerative process (e.g., failure to repair myelin damage [Connor et al., 1990] or to a neurodevelopmental process (abnormal brain development and myelination [Nopoulos et al., 2010]) has still not been clarified. Perhaps a more dynamic approach, connecting both aspects (neurodegenerative and neurodevelopmental), would be useful to better understand the iron mechanism. Once again, we cite the hypothesis proposed by Bartzokis [Bartzokis et al., 2007], according to which the HD brain may be continually trying to remyelinate in a losing attempt to compensate for the disease-related myelin loss (neurodegenerative aspect). In HD, these remyelination processes may successfully compensate in younger years but then start to fail in older years as the brain myelin volume continues to grow and it becomes increasingly difficult to maintain this expanding volume. This is similar to what happens in healthy older individuals [Bartzokis et al., 2012]. The early and continuous expenditure of resources to repair myelin might support these data, by suggesting some slowing in brain development (neurodevelopmental aspect).

Longitudinal studies of juvenile forms of HD would help verify whether myelin breakdown and changes in iron levels are causal factors in HD pathogenesis and when in the course of pathology they start to act. Moreover, early intervention to reduce myelin breakdown and correct iron accumulation might make it possible to increase effectiveness of treatment, decrease the need for later more aggressive approaches, and ultimately might represent a heretofore unexplored opportunity for primary prevention of degenerative brain diseases [Bartzokis, 2005; Nguyen et al., 2005; Youdim et al., 2004].

REFERENCES

Ashburner J, Friston KJ (2000): Voxel-based morphometry—The methods. Neuroimage 11(6 Part 1):805–821.

Bartzokis G (2005): Brain myelination in prevalent neuropsychiatric developmental disorders: Primary and comorbid addiction. Adolesc Psychiatry 29:55–96.

Bartzokis G, Cummings J, Perlman S, Hance DB, Mintz J (1999): Increased basal ganglia iron levels in Huntington disease. Arch Neurol 56:569–574.

Bartzokis G, Lu PH, Tishler TA, Fong SM, Oluwadara B, Finn JP, Huang D, Bordelon Y, Mintz J, Perlman S (2007): Myelin breakdown and iron changes in Huntington's disease: Pathogenesis and treatment implications. Neurochem Res 32:1655–1664.

Bartzokis G, Lu PH, Heydari P, Couvrette A, Lee GJ, Kalashyan G, Freeman F, Grinstead JW, Villablanca P, Finn JP, Mintz J, Alger JR, Altshuler LL (2012): Multimodal magnetic resonance imaging assessment of white matter aging trajectories over the lifespan of healthy individuals. Biol Psychiatry 72:1026–1034.

Bartzokis G, Tishler TA (2000): MRI evaluation of basal ganglia ferritin iron and neurotoxicity in Alzheimer's and Huntingon's disease. Cell Mol Biol (Noisy-le-grand) 46:821–833.

Beal MF (1996): Mitochondria, free radicals, and neurodegeneration. Curr Opin Neurobiol 6:661–666.

Cherubini A, Peran P, Caltagirone C, Sabatini U, Spalletta G (2009): Aging of subcortical nuclei: Microstructural, mineralization and atrophy modifications measured in vivo using MRI. Neuroimage 48:29–36.

Connor JR, Menzies SL, St Martin SM, Mufson EJ (1990): Cellular distribution of transferrin, ferritin, and iron in normal and aged human brains. J Neurosci Res 27:595–611.

Deichmann R, Schwarzbauer C, Turner R (2004): Optimisation of the 3D MDEFT sequence for anatomical brain imaging: Technical implications at 1.5 and 3 T. Neuroimage 21:757–767.

Di Paola M, Luders E, Cherubini A, Sanchez-Castaneda C, Thompson PM, Toga AW, Caltagirone C, Orobello S, Elifani F, Squitieri F, Sabatini U (2012): Multimodal MRI analysis of the corpus callosum reveals white matter differences in presymptomatic and early Huntington's disease. Cereb Cortex 22:2858–2866.

Folstein MF, Folstein SE, McHugh PR (1975): "Mini-mental state". A practical method for grading the cognitive state of patients for the clinician. J Psychiatr Res 12:189–198.

Good CD, Johnsrude IS, Ashburner J, Henson RN, Friston KJ, Frackowiak RS (2001): A voxel-based morphometric study of ageing in 465 normal adult human brains. Neuroimage 14(1 Part 1):21–36.

He X, Yablonskiy DA (2009): Biophysical mechanisms of phase contrast in gradient echo MRI. Proc Natl Acad Sci USA 106: 13558–13563.

Hilditch-Maguire P, Trettel F, Passani LA, Auerbach A, Persichetti F, MacDonald ME (2000): Huntingtin: An iron-regulated protein essential for normal nuclear and perinuclear organelles. Hum Mol Genet 9:2789–2797.

Hobbs NZ, Henley SM, Ridgway GR, Wild EJ, Barker RA, Scahill RI, Barnes J, Fox NC, Tabrizi SJ (2010): The progression of regional atrophy in premanifest and early Huntington's disease: A longitudinal voxel-based morphometry study. J Neurol Neurosurg Psychiatry 81:756–763.

Huntington, Study, Group. (1996): Unified Huntington's Disease Rating Scale: Reliability and consistency. Mov Disord 11:136–142.

Koeppen AH (1995): The history of iron in the brain. J Neurol Sci 134:1–9.

LeVine SM, Macklin WB (1990): Iron-enriched oligodendrocytes: A reexamination of their spatial distribution. J Neurosci Res 26:508–512.

Li W, Wu B, Avram AV, Liu C (2012): Magnetic susceptibility anisotropy of human brain in vivo and its molecular underpinnings. Neuroimage 59:2088–2097.

Moos T, Morgan EH (2004): The metabolism of neuronal iron and its pathogenic role in neurological disease: Review. Ann NY Acad Sci 1012:14–26.

Nguyen T, Hamby A, Massa SM (2005): Clioquinol down-regulates mutant huntingtin expression in vitro and mitigates pathology in a Huntington's disease mouse model. Proc Natl Acad Sci USA 102:11840–11845.

Nichols TE, Holmes AP (2002): Nonparametric permutation tests for functional neuroimaging: A primer with examples. Hum Brain Mapp 15:1–25.

Nopoulos PC, Aylward EH, Ross CA, Johnson HJ, Magnotta VA, Juhl AR, Pierson RK, Mills J, Langbehn DR, Paulsen JS (2010): Cerebral cortex structure in prodromal Huntington disease. Neurobiol Dis 40:544–554.

Paulsen JS, Zhao H, Stout JC, Brinkman RR, Guttman M, Ross CA, Como P, Manning C, Hayden MR, Shoulson I (2001): Clinical markers of early disease in persons near onset of Huntington's disease. Neurology 57:658–662.

Penney JB, Vonsattel JP, MacDonald ME, Gusella JF, Myers RH (1997): CAG repeat number governs the development rate of pathology in Huntington's disease. Ann Neurol 41:689–692.

Peran P, Cherubini A, Luccichenti G, Hagberg G, Demonet JF, Rascol O, Celsis P, Caltagirone C, Spalletta G, Sabatini U (2009): Volume and iron content in basal ganglia and thalamus. Hum Brain Mapp 30:2667–2675.

Rosas HD, Lee SY, Bender AC, Zaleta AK, Vangel M, Yu P, Fischl B, Pappu V, Onorato C, Cha JH, Salat DH, Hersch SM (2010): Altered white matter microstructure in the corpus callosum in Huntington's disease: Implications for cortical "disconnection". Neuroimage 49:2995–3004.

Salvador GA, Uranga RM, Giusto NM (2011): Iron and mechanisms of neurotoxicity. Int J Alzheimers Dis 720658.

Sánchez-Castañeda C, Cherubini A, Elifani F, Péran P, Orobello S, Capelli G, Sabatini U, Squitieri F (2013): Seeking Huntington disease biomarkers by multimodal, cross-sectional basal ganglia imaging. Hum Brain Mapp 34:1625–1635.

Schulz K, Vulpe CD, Harris LZ, David S (2011): Iron efflux from oligodendrocytes is differentially regulated in gray and white matter. J Neurosci 31:13301–13311.

Smith SM, Jenkinson M, Johansen-Berg H, Rueckert D, Nichols TE, Mackay CE, Watkins KE, Ciccarelli O, Cader MZ, Matthews PM, Behrens TE (2006): Tract-based spatial statistics: Voxelwise analysis of multi-subject diffusion data. Neuroimage 31:1487–1505.

Specht K, Minnerop M, Muller-Hubenthal J, Klockgether T (2005): Voxel-based analysis of multiple-system atrophy of cerebellar type: Complementary results by combining voxel-based morphometry and voxel-based relaxometry. Neuroimage 25:287–293.

Thomas M, Jankovic J (2004): Neurodegenerative disease and iron storage in the brain. Curr Opin Neurol 17:437–442.

Todorich B, Pasquini JM, Garcia CI, Paez PM, Connor JR (2009): Oligodendrocytes and myelination: The role of iron. Glia 57: 467–478.

Vonsattel JP, Keller C, Del Pilar Amaya M (2008): Neuropathology of Huntington's disease. In: Duyckaerts C, Litvan I, editors. Handbook of Clinical Neurology Amsterdam: Elsevier. pp 599–618.

Yablonskiy DA, Haacke EM (1994): Theory of NMR signal behavior in magnetically inhomogeneous tissues: The static dephasing regime. Magn Reson Med 32:749–763.

Youdim MB, Stephenson G, Ben Shachar D (2004): Ironing iron out in Parkinson's disease and other neurodegenerative diseases with iron chelators: A lesson from 6-hydroxydopamine and iron chelators, desferal and VK-28. Ann NY Acad Sci 1012:306–325.

Zecca L, Youdim MB, Riederer P, Connor JR, Crichton RR (2004): Iron, brain ageing and neurodegenerative disorders. Nat Rev Neurosci 5:863–873.